

Purcell-enhanced emissions from diamond color centers in slow light photonic crystal waveguides

Sophie W. Ding^{1, #, †}, Chang Jin^{1, #}, Kazuhiro Kuruma^{1, 2, #, *}, Xinghan Guo³, Michael Haas¹, Boris Korzh⁴, Andrew Beyer⁴, Matt Shaw⁴, Neil Sinclair¹, David D. Awschalom^{3, 5}, F. Joseph Heremans^{3, 5}, Nazar Deegan⁵, Alexander A. High^{3, 5, *}, and Marko Loncar^{1, *}

¹John A. Paulson School of Engineering and Applied Sciences, Harvard University, Cambridge, Massachusetts, USA.

²Research Center for Advanced Science and Technology, The University of Tokyo, Meguro-ku, Tokyo, Japan.

³Pritzker School of Molecular Engineering, University of Chicago, Chicago, IL, USA.

⁴Jet Propulsion Laboratory, California Institute of Technology, 4800 Oak Grove Dr., Pasadena, California 91109, USA

⁵Q-NEXT, Argonne National Laboratory, Lemont, IL.

*E-mail: kkuruma@g.ecc.u-tokyo.ac.jp; ahigh@uchicago.edu; loncar@g.harvard.edu

#These authors contributed equally: Sophie W. Ding, Chang Jin, Kazuhiro Kuruma.

†Present address: AWS Center for Quantum Computing, San Francisco, California, USA.

Abstract

Quantum memories based on emitters with optically addressable spins rely on efficient photonic interfaces, often implemented as nanophotonic cavities with ideally narrow spectral linewidths and small mode volumes. However, these approaches require nearly perfect spectral and spatial overlap between the cavity mode and quantum emitter, which can be challenging. This is especially true in the case of solid-state quantum emitters that are often randomly positioned and can suffer from significant inhomogeneous broadening. An alternative approach to mitigate these challenges is to use slow-light waveguides that can enhance light-matter interaction across large optical bandwidths and large areas. Here, we demonstrate diamond slow light photonic crystal (PhC) waveguides that enable broadband optical coupling to embedded silicon-vacancy (SiV) color centers. We take advantage of the recently demonstrated thin-film diamond photonic platform to fabricate fully suspended two-dimensional PhC waveguides. Using this approach, we demonstrate waveguide modes with high group indices up to 70 and observe Purcell-enhanced emissions of the SiVs coupled to the waveguide mode. Our approach represents a practical diamond platform for robust spin-photon interfaces with color centers.

Introduction

Color centers in diamond have emerged as promising platforms for quantum information processing, and have been used as single photon sources¹⁻³, as well as quantum memories by leveraging their long-lived and optically accessible spins^{45,64}. Additionally, they play an important role in scalable quantum networks, where long-distance entanglement between multiple color centers has been demonstrated⁷⁻⁹. For practical quantum applications, achieving high emission rates and collection efficiencies of emitted photons are key. As a result, a wide variety of diamond nanophotonic structures have been explored, including optical cavities¹⁰⁻¹³. Among them, diamond PhC cavities, with their small mode volumes (V) and relatively high quality factors (Q)¹⁴⁻¹⁶, are considered the most promising and have been the workhorses behind various quantum network demonstrations^{5,6}.

However, large Q and small V put stringent constraints on the spectral and spatial overlap between the color center and the cavity mode, which can be challenging to achieve. For example, fabrication tolerances can significantly affect the resonant wavelength of the fabricated cavities, while variations in the local environment of each emitter (e.g. strain, charge, etc) can result in inhomogeneous broadening^{17,18}. While spatial mismatch can be addressed using techniques based on deterministic positioning of color centers in nanostructures^{19,20}, the spectral mismatch requires tuning either the cavity resonance, e.g. using gas condensation^{21,22} or surface oxidation/deposition^{11,14,23}, or the emitter, e.g. by strain^{24,25}. These, however, can be challenging to implement in a scalable manner^{26,27}.

An alternative approach to achieve an efficient photonic interface is to use slow light waveguides. Slow light PhC waveguides can enable broadband optical coupling to solid-state emitters as well as enhance spontaneous emission of the emitters by the Purcell effect in the slow light region²⁸⁻³¹, leading to near-unity cavity-emitter coupling efficiency (β)³². PhC waveguides can also allow for chiral coupling to quantum emitters with circularly polarized emissions³³, as well as enable efficient topologically-protected nanophotonic devices^{34,35}. Two-dimensional (2D) PhC waveguides could also offer better thermalization and optical power handling³⁶, which are critical for the required cryogenic temperature for quantum operation. Despite these advantages, 2D slow light PhC waveguides in diamond or their coupling to color centers have not been demonstrated. This is likely due to the fabrication challenges associated with fabricating suspended 2D diamond devices compatible with color centers.

Here, we demonstrate 2D slow light PhC waveguides coupled to silicon-vacancy centers (SiVs) in diamond. We fabricate the PhC waveguides on a single crystalline thin film diamond created by scalable fabrication techniques with a combination of ion implantation, diamond overgrowth, and

thin film transfer-printing processes^{37,38}. We show high group indices (n_g) up to 70 in the slow-light regime through photoluminescence measurements of the waveguide modes. We also observe Purcell-enhanced emission from (single) SiVs coupled to the PhC waveguide mode, with a ~ 2 -fold increase in the spontaneous emission rate in the slow-light regime compared to those in the slab. These findings present a scalable pathway for efficient quantum photonic platforms with diamond color centers.

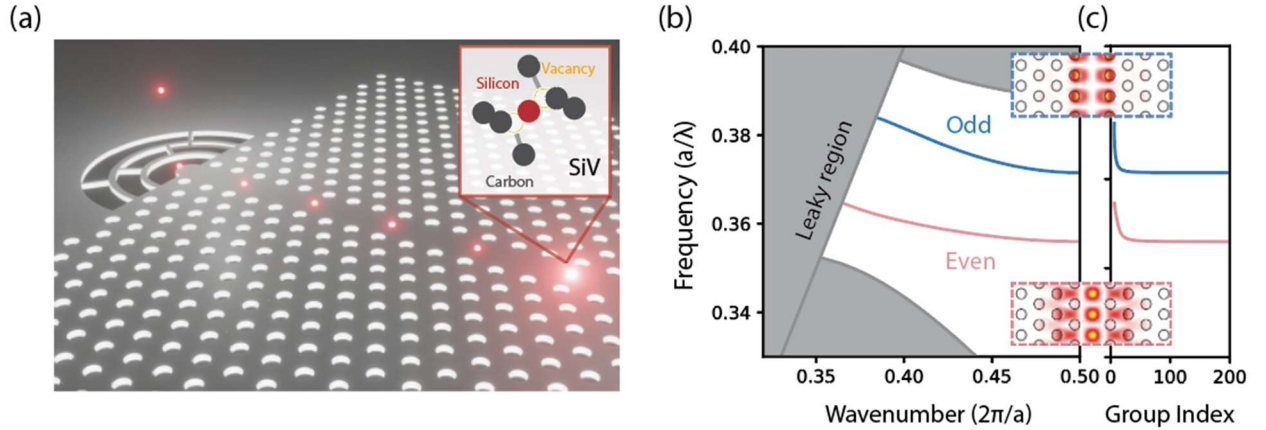


Fig. 1. (a) A schematic view of a suspended PhC diamond waveguide with embedded (single) SiVs. Input/output grating couplers are located at both ends of the waveguide (only one side is shown in the figure). The red dots signify the photons emitted by the SiV guided by the waveguide and coupled out through the grating coupler. (b) Simulated dispersion relation for the slow-light waveguide. Red and blue curves are even (0th-order) and odd (1st-order) modes, respectively. a is the lattice constant of the photonic crystal. (c) Corresponding group index of the two modes. The insets show the simulated electric field ($|E_y|^2$) profiles of the even and odd modes with n_g of ~ 20 at $0.357(a/\lambda)$ and $0.373(a/\lambda)$, respectively.

As schematically shown in Fig. 1(a), the diamond PhC waveguide is formed by removing one row in the 2D PhCs. We vary the lattice constants in fabrication, where $a=255-275$ nm and an air hole radius (r) of 65 nm. The thickness of the diamond slab (d) is 160 nm. Fig. 1(b) shows the band diagram for the PhC waveguide calculated using the 3D plane wave expansion (PWE) method. The refractive index of the diamond slab is assumed to be $n = 2.4$. Two distinct guided waveguide modes are found inside the photonic bandgap, spanning the frequency range $a/\lambda = 0.353-0.389$, where λ is the wavelength. The lower frequency waveguide mode corresponds to the even (0th-order) mode (lower inset), while the higher frequency mode is the odd (1st-order) waveguide mode

(upper inset). The band structure of these waveguide modes is consistent with previous reports using PhC waveguides^{30,39}. Fig. 1(c) shows the calculated group index (n_g), obtained by $n_g = c(dk/d\omega)$, using the data from Fig. 1(b). For both modes, group indices exceeding 100 can be found near the edge of Brillouin zone. In our experiments, we focus on the even waveguide mode to demonstrate coupling with SiVs.

We fabricate the designed waveguide on a 160 nm-thick diamond membrane with a surface roughness < 0.3 nm and thickness variation of ~ 1 nm. The detailed fabrication and properties of the diamond membrane can be found in previous work^{37,38}. Fig. 2(a) shows the simplified flow of the fabrication process¹⁶. The diamond membrane ($200 \mu\text{m} \times 200 \mu\text{m}$) is implanted with Si ions resulting in randomly positioned SiVs. The implantation depth is 40 nm below the diamond surface. The membrane is transferred onto a SiO₂-on-Si substrate ($10 \text{ mm} \times 10 \text{ mm}$) by a transfer-printing technique for handling (step 1). Next, we deposit Au/Cr at the edges of the membrane via a liftoff process to secure the membrane and minimize the chances of delamination during the fabrication process (step 2). We then deposit 100 nm-thick SiN and 400 nm-thick electron beam (EB) resist (ZEP-520A) on the membrane (step 3). EB lithography is used to write the waveguide structure, which is then transferred into the SiN mask layer by inductively coupled plasma reactive ion etching (ICP-RIE) using SF₆ and C₄F₈ gases (step 4). We then transfer the waveguide pattern from the mask into the diamond membrane using O₂-plasma RIE (step 5). The SiN and SiO₂ layers are removed by immersion in hydrofluoric acid (HF). Finally, we perform additional undercutting using XeF₂ gas to etch the Si substrate underneath to maintain enough air gap between the diamond slab and Si substrate (step 6).

An optical microscope image of the diamond membrane with fabricated arrays of PhC waveguides is shown in Fig. 2(b). Fig. 2(c) shows the top view of a scanning electron microscope (SEM) image of a fabricated PhC waveguide. The position of grating couplers is slightly shifted from the center of the waveguide to increase the visibility of Fabry-Perot (FP) fringes³⁴ (Fig. 2(c)). Fig. 2(d) and (e) display the zoom-in view of the PhC waveguide and grating coupler region, respectively. We emphasize that our fabrication method does not involve complicated bulk diamond undercut processes that can result in additional surface roughness^{40,41}. This is critical for realizing high-quality photonic devices in diamond¹⁶, especially those based on 2D photonic crystal structures.

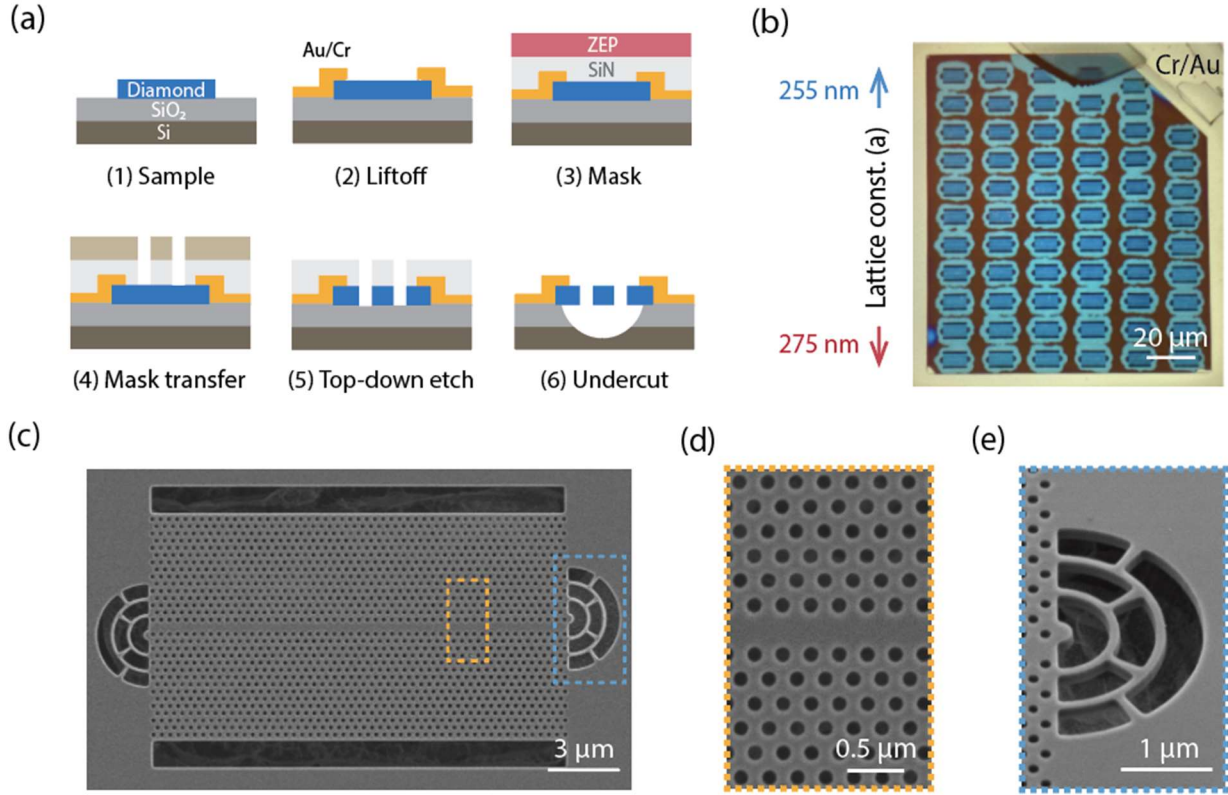


Fig. 2. (a) Process flow for fabrication of PhC waveguides in a thin film diamond: (1) thin film diamond is transferred onto SiO₂/Si substrate; (2) Au/Cu pad is created around the diamond by a liftoff process; (3) EB resist (ZEP-520A) and SiN layer are formed on the diamond; (4) the pattern on the EB resist is transferred unto the SiN mask; (5) the waveguide structure is patterned into the diamond by ICP-RIE-based top-down etching; (6) The undercut process is performed by etching SiO₂ and Si underneath. (b) Optical microscope image of a fabricated PhC waveguide array in a thin film diamond (200 × 200 μm) on a Si substrate. The thin film is secured on the Si substrate with Au/Cr pads. (c) SEM images of one of the fabricated PhC waveguides. The grating couplers are positioned at each waveguide end, and are intentionally misaligned from the waveguide. This forms a low Q FP cavity between two grating couplers, which helps with the estimation of group indices (Fig. 3). Zoom-in views of the (d) waveguide and (e) grating coupler regions.

We first perform photoluminescence (PL) measurements to optically characterize the fabricated PhC waveguides at room temperature (Fig. 3), leveraging the background emissions of nitrogen-vacancy centers formed during the diamond thin film overgrowth process³⁷ as internal sources. We couple 532 nm continuous-wave light into a waveguide by focusing it to one waveguide end and collect PL signal generated in the waveguide using the same grating coupler. The collected signal is analyzed by a spectrometer and shown in Fig. 3 (a). We show the PL spectra of fabricated waveguides with three different lattice constants of $a = 257, 259,$ and 261 nm. We observe sharp

FP fringes formed by the light reflection at both grating couplers³⁴ for both even and odd modes, around 730 nm and 690 nm, respectively. The wavelengths of these modes increase as a increases, as expected. The SiV emission peak is also seen around 737 nm (indicated by the gray dashed line). Fig. 3 (b) displays the enlarged view of the PL spectrum for $a = 261$ nm, confirming that the FP fringes of the even waveguide mode (ranging from 715-740 nm) overlap with the SiV emission peak. The fringe spacing decreases as the peak wavelength increases (Fig. 3(b)), indicating that the n_g increases near the Brillouin zone edge of the waveguide mode due to the reduced group velocity. From the observed FP fringes, we estimate n_g for the fabricated waveguide using the following equation: $n_g = \lambda / 2L\Delta\lambda^2$. Here, L is the waveguide length of $51a$ while λ and $\Delta\lambda$ are the center wavelength of the FP peak and the wavelength difference between two adjacent FP peaks, respectively. The wavelengths of FP peaks are extracted by fitting the PL spectrum with multiple Lorentzian peak functions. Fig. 3(c) shows the measured n_g overlaid with the simulated values (dash line), with the largest measured value being $n_{g,max} = 73$. For comparison between simulated and experimental n_g , we ascribe a wavelength offset to the simulated n_g (Fig.1(c)) to compensate for the wavelength differences caused by fabrication imperfection. The simulated n_g with the offset is in good agreement with the experimental data. It is worth noting that the linewidth of the fringe peaks (corresponding to the quality factor) becomes narrower (higher) as it approaches the slow light region (Fig. 3(b)) (supplementary information), which is consistent with previous observations in PhC waveguides^{31,34}. These results indicate the successful demonstration of slow light PhC waveguides in diamond.

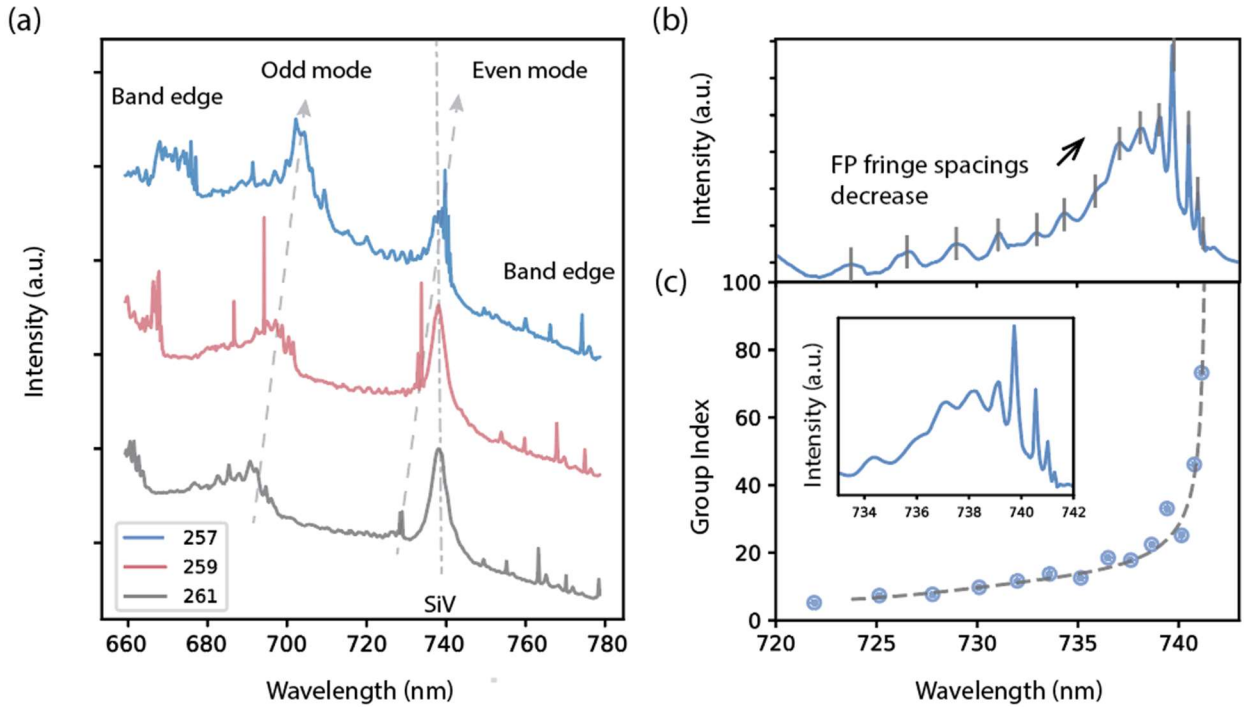


Fig. 3. (a) PL spectra measured at room temperature for fabricated waveguides with three different lattice constants ($a=257, 259, 261$ nm). Peaks at 738 nm correspond to the SiV emission (gray

dash line). The gray arrows indicate the positions of odd and even waveguide modes as they shift with the lattice constant. (b) PL spectrum of a waveguide with $a = 261$ nm shown in (a), after subtracting the broad background fitted by a Gaussian function. (c) Extracted group indices from the spectrum of the FP fringes in (b), obtained by fitting with multiple Lorentz functions. The inset shows the zoom-in view around the slow light region corresponding to (b). The dashed gray curve corresponds to the calculated group indices with a wavelength offset for comparison with the experimental data.

Finally, we perform PL measurements at 5 K (see supplementary information) to investigate the coupling between the PhC waveguide modes and the SiVs (see supplementary information). The SiVs in the waveguide are pumped from above by 520 nm laser light (green arrow in Fig. 4 (a)), and SiV emissions transmitted through the waveguide are collected from one of the grating couplers (red arrow in Fig. 4 (a)) or from free-space. For the optical coupling to SiVs, we use PhC waveguides with $a = 261$ nm, which has an overlap between the even waveguide modes and the SiV emission, as shown in Fig. 3 (b). Figure 4 (b) shows an energy diagram of the SiVs with four possible optical transitions (A-D). An example of the emission spectrum for a SiV measured from one of the grating couplers is shown in Fig. 4(c), exhibiting the four sharp peaks corresponding to the A-D transitions (see Fig. 4(b)). The observation of SiV emissions via the grating coupler suggests that the SiV is optically coupled to the waveguide mode. We then conduct lifetime measurements on the same SiV using a pulsed laser (supplementary information). The SiV emission is collected at the same spot as the laser excitation spot. We use a spectral filter with a bandwidth of ~ 50 GHz to filter out only the B or C transition around 737 nm. Based on the measured n_g for the waveguide devices (see supplementary information), we estimate the n_g experienced by the SiVs to be in the range of 11-20. This variation in n_g between different waveguides can be attributed to fabrication imperfections. Figure 4(d) shows the shortest lifetime (1.01 ± 0.05 ns, blue, measured at $n_g = 11$) measured in a waveguide, compared to the longest lifetime (2.32 ± 0.12 ns, red) measured in a slab. The decay is fitted with a single exponential with a background offset (black dashed lines). Compared to a typical lifetime of SiV in bulk (~ 1.7 ns)^{21,42}, the observed lifetime in a waveguide is reduced by a factor of ~ 1.7 . These observations of the lifetime reduction suggest the spontaneous emission rate of the SiV is enhanced by the Purcell effect in the slow light region. We also statistically investigate the enhancement of the SiV emission coupled to waveguide modes. Fig. 4(e) shows the comparison of lifetime measurements for several SiVs located in two different waveguides with the same structure parameters and on the slab. Overall, the SiV lifetimes in the waveguides (average to 1.30 ns, red star) are shorter than the typical SiV lifetime due to the slow light effect, while those in the slab tend to be the same or longer than bulk SiVs (average to 1.83 ns, blue star). The longer lifetimes in the slab likely are due to the reduced photonic density of states by the slab structure.

The Purcell factor (F_{ZPL}) for the investigated ZPL with a lifetime at high n_g region is estimated to be up to ~ 2.2 (see supplementary information), in good agreement with the simulated value of ~ 2.5 (see supplementary information). We also estimate a waveguide-emitter coupling efficiency (β) of $\sim 72\%$ for the shortest lifetime of 1.0 ns (supplementary information). This value is smaller than values reported in a good cavity-SiV coupled system²¹ because of its smaller Purcell enhancement. However, we note that the broadband nature of our devices can allow Purcell enhancement of multiple SiVs without the need for spectral tuning, as is the case in cavity-SiV coupled systems. Our theoretical estimation suggests further optimization, including better spatial matching, could enable $\beta \sim 94\%$ with the experimentally achieved $n_g \sim 70$ (see supplementary information)

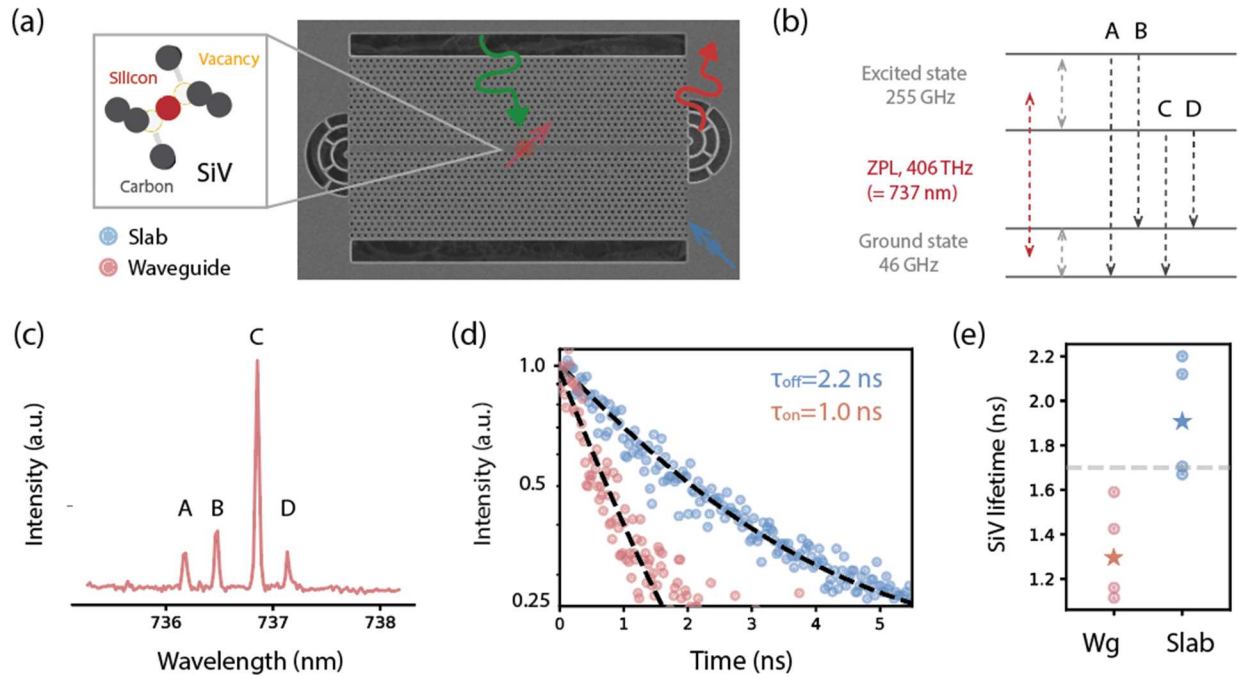


Fig. 4. (a) SEM image of a fabricated waveguide. The positions of the excitation and detection are indicated as green arrows and red arrows for measuring the PL spectrum of SiVs. (b) Energy levels of an SiV with 4 possible optical transitions (A~D). (c) PL spectrum of an SiV in the PhC waveguide measured via one of the grating couplers. (d) PL lifetimes of the SiV B and/or C transition in waveguides (red) and in the slab the membrane (blue). The dashed lines correspond to fitting curves with a single exponential function with an offset. (e) Summary of different SiV lifetimes, measured using B and/or C transition: four SiVs are measured in two different waveguides with $a = 261$ nm and four in the diamond slab. The round dots are the measured data points, and the star dots are the average values of all the waveguide and slab SiV lifetime. The dashed line is the nominal bulk SiV lifetime of 1.7 ns at 4 K.

In summary, we demonstrate slow light 2D PhC waveguides in diamond and study their effect on the emission properties of SiVs. The waveguide modes show a high n_g up to ~ 70 in the slow light regime. We observe Purcell-enhanced emissions from SiVs in slow-light PhC waveguides, with shorter SiV lifetimes compared to typical bulk ones. Our slow light PhC waveguide approach can be applied to color centers in not only diamond but also other quantum photonic materials, such as silicon carbide⁴³ and silicon⁴⁴. The proposed fabrication method and PhC waveguide design can also be used to realize more advanced diamond photonic structures, such as chiral waveguide interfaces and topological devices³⁵, in combination with quantum emitters. Our demonstrations pave the road towards developing novel and efficient photonic hardware for quantum networks based on the color center in diamond.

Acknowledgments

We would like to thank Prof. S. Iwamoto for the technical support. This work was supported by AFOSR (Grant No. FA9550-19-1-0376, and FA9550-20-1-0105), ARO MURI (Grant No. W911NF1810432), NSF RAISE TAQS (Grant No. ECCS-1838976), NSF STC (Grant No. DMR-1231319), NSF ERC (Grant No. EEC-1941583), DOE (Grant No. DE-SC0020376), DFG SFB 1375 “NOA” project C5, and ONR (Grant No. N00014-20-1-2425), a research grant from The Mazda Foundation. This work was performed in part at the Center for Nanoscale Systems (CNS), Harvard University. The low-jitter SNSPDs were fabricated at the Jet Propulsion Laboratory, California Institute of Technology, under a contract with the National Aeronautics and Space Administration. Diamond membrane synthesis is based upon work primarily supported by the U.S. Department of Energy Office of Science National Quantum Information Science Research Centers as part of the Q-NEXT center.

References

- (1) Kurtsiefer, C.; Mayer, S.; Zarda, P.; Weinfurter, H. Stable Solid-State Source of Single Photons. *Phys. Rev. Lett.* **2000**, *85* (2), 290–293.
- (2) Babinec, T. M.; Hausmann, B. J. M.; Khan, M.; Zhang, Y.; Maze, J. R.; Hemmer, P. R.; Lončar, M. A Diamond Nanowire Single-Photon Source. *Nat. Nanotechnol.* **2010**, *5* (3), 195–199.
- (3) Knall, E. N.; Knaut, C. M.; Bekenstein, R.; Assumpcao, D. R.; Stroganov, P. L.; Gong, W.; Huan, Y. Q.; Stas, P.-J.; Machielse, B.; Chalupnik, M.; Levonian, D.; Suleymanzade, A.; Riedinger, R.; Park, H.; Lončar, M.; Bhaskar, M. K.; Lukin, M. D. Efficient Source of Shaped Single Photons Based on an Integrated Diamond Nanophotonic System. *Phys. Rev. Lett.* **2022**, *129* (5), 053603–053603.
- (4) Maurer, P. C.; Kucsko, G.; Latta, C.; Jiang, L.; Yao, N. Y.; Bennett, S. D.; Pastawski, F.; Hunger, D.; Chisholm, N.; Markham, M.; Twitchen, D. J.; Cirac, J. I.; Lukin, M. D. Room-Temperature Quantum Bit Memory Exceeding One Second. *Science* **2012**, *336* (6086), 1283–1286.

- (5) Bhaskar, M. K.; Riedinger, R.; Machielse, B.; Levonian, D. S.; Nguyen, C. T.; Knall, E. N.; Park, H.; Englund, D.; Lončar, M.; Sukachev, D. D.; Lukin, M. D. Experimental Demonstration of Memory-Enhanced Quantum Communication. *Nature* **2020**, *580* (7801), 60–64.
- (6) Knaut, C. M.; Suleymanzade, A.; Wei, Y.-C.; Assumpcao, D. R.; Stas, P.-J.; Huan, Y. Q.; Machielse, B.; Knall, E. N.; Sutula, M.; Baranes, G.; Sinclair, N.; De-Eknamkul, C.; Levonian, D. S.; Bhaskar, M. K.; Park, H.; Lončar, M.; Lukin, M. D. Entanglement of Nanophotonic Quantum Memory Nodes in a Telecom Network. *Nature* **2024**, *629* (8012), 573–578.
- (7) Kalb, N.; Reiserer, A. A.; Humphreys, P. C.; Bakermans, J. J. W.; Kamerling, S. J.; Nickerson, N. H.; Benjamin, S. C.; Twitchen, D. J.; Markham, M.; Hanson, R. Entanglement Distillation between Solid-State Quantum Network Nodes. *Science* **2017**, *356* (6341), 928–932.
- (8) Pompili, M.; Hermans, S. L. N.; Baier, S.; Beukers, H. K. C.; Humphreys, P. C.; Schouten, R. N.; Vermeulen, R. F. L.; Tiggelman, M. J.; dos Santos Martins, L.; Dirkse, B.; Wehner, S.; Hanson, R. Realization of a Multinode Quantum Network of Remote Solid-State Qubits. *Science* **2021**, *372* (6539), 259–264.
- (9) Hermans, S. L. N.; Pompili, M.; Beukers, H. K. C.; Baier, S.; Borregaard, J.; Hanson, R. Qubit Teleportation between Non-Neighbouring Nodes in a Quantum Network. *Nature* **2022**, *605* (7911), 663–668.
- (10) Faraon, A.; Barclay, P. E.; Santori, C.; Fu, K.-M. C.; Beausoleil, R. G. Resonant Enhancement of the Zero-Phonon Emission from a Colour Centre in a Diamond Cavity. *Nat. Photonics* **2011**, *5* (5), 301–305.
- (11) Riedrich-Möller, J.; Kipfstuhl, L.; Hepp, C.; Neu, E.; Pauly, C.; Mücklich, F.; Baur, A.; Wandt, M.; Wolff, S.; Fischer, M.; Gsell, S.; Schreck, M.; Becher, C. One-and Two-Dimensional Photonic Crystal Microcavities in Single Crystal Diamond. *Nat. Nanotechnol.* **2012**, *7* (1), 69–74.
- (12) Hausmann, B. J. M.; Shields, B.; Quan, Q.; Maletinsky, P.; McCutcheon, M.; Choy, J. T.; Babinec, T. M.; Kubanek, A.; Yacoby, A.; Lukin, M. D.; Loncar, M. Integrated Diamond Networks for Quantum Nanophotonics. *Nano Lett.* **2012**, *12* (3), 1578–1582.
- (13) Albrecht, R.; Bommer, A.; Deutsch, C.; Reichel, J.; Becher, C. Coupling of a Single Nitrogen-Vacancy Center in Diamond to a Fiber-Based Microcavity. *Phys. Rev. Lett.* **2013**, *110* (24), 243602–243602.
- (14) Hausmann, B. J. M.; Shields, B. J.; Quan, Q.; Chu, Y.; de Leon, N. P.; Evans, R.; Burek, M. J.; Zibrov, A. S.; Markham, M.; Twitchen, D. J.; Park, H.; Lukin, M. D.; Lončar, M. Coupling of NV Centers to Photonic Crystal Nanobeams in Diamond. *Nano Lett.* **2013**, *13* (12), 5791–5796.
- (15) Burek, M. J.; Chu, Y.; Liddy, M. S. Z.; Patel, P.; Rochman, J.; Meesala, S.; Hong, W.; Quan, Q.; Lukin, M. D.; Lončar, M. High Quality-Factor Optical Nanocavities in Bulk Single-Crystal Diamond. *Nat. Commun.* **2014**, *5* (1), 5718–5718.
- (16) Ding, S. W.; Haas, M.; Guo, X.; Kuruma, K.; Jin, C.; Li, Z.; Awschalom, D. D.; Deegan, N.; Heremans, F. J.; High, A.; Loncar, M. High-Q Cavity Interface for Color Centers in Thin Film Diamond. *Nat. Commun.* **2024**, No. February. <https://doi.org/10.1038/s41467-024-50667-5>.
- (17) Evans, R. E.; Sipahigil, A.; Sukachev, D. D.; Zibrov, A. S.; Lukin, M. D. Narrow-Linewidth Homogeneous Optical Emitters in Diamond Nanostructures via Silicon Ion Implantation. *Phys. Rev. Appl.* **2016**, *5* (4), 044010–044010.
- (18) Pregnolato, T.; Stucki, M. E.; Bopp, J. M.; v. d. Hoeven, M. H.; Gokhale, A.; Krüger, O.; Schröder, T. Fabrication of Sawfish Photonic Crystal Cavities in Bulk Diamond. *APL Photonics* **2024**, *9* (3), 036105.
- (19) Sipahigil, A.; Evans, R. E.; Sukachev, D. D.; Burek, M. J.; Borregaard, J.; Bhaskar, M. K.; Nguyen, C. T.; Pacheco, J. L.; Atikian, H. A.; Meuwly, C.; Camacho, R. M.; Jelezko, F.; Bielejec, E.; Park, H.; Lončar, M.; Lukin, M. D. An Integrated Diamond Nanophotonics Platform for Quantum-Optical Networks. *Science* **2016**, *354* (6314), 847–850.
- (20) Schröder, T.; Walsh, M.; Zheng, J.; Mouradian, S.; Li, L.; Malladi, G.; Bakhru, H.; Lu, M.; Stein, A.; Heuck, M.; Englund, D. Scalable Fabrication of Coupled NV Center - Photonic Crystal Cavity Systems by Self-Aligned N Ion Implantation. *Opt. Mater. Express* **2017**, *7* (5), 1514–1514.

- (21) Zhang, J. L.; Sun, S.; Burek, M. J.; Dory, C.; Tzeng, Y.-K.; Fischer, K. A.; Kelaita, Y.; Lagoudakis, K. G.; Radulaski, M.; Shen, Z.-X.; Melosh, N. A.; Chu, S.; Lončar, M.; Vučković, J. Strongly Cavity-Enhanced Spontaneous Emission from Silicon-Vacancy Centers in Diamond. *Nano Letters* **2018**, *18* (2), 1360–1365.
- (22) Kuruma, K.; Pingault, B.; Chia, C.; Renaud, D.; Hoffmann, P.; Iwamoto, S.; Ronning, C.; Lončar, M. Coupling of a Single Tin-Vacancy Center to a Photonic Crystal Cavity in Diamond. *Appl. Phys. Lett.* **2021**, *118* (23), 230601–230601.
- (23) Fait, J.; Varga, M.; Hruška, K.; Kromka, A.; Rezek, B.; Ondič, L. Spectral Tuning of Diamond Photonic Crystal Slabs by Deposition of a Thin Layer with Silicon Vacancy Centers. *Nanophotonics* **2021**, *10* (15), 3895–3905.
- (24) Sohn, Y.-I.; Meesala, S.; Pingault, B.; Atikian, H. A.; Holzgrafe, J.; Gündoğan, M.; Stavrakas, C.; Stanley, M. J.; Sipahigil, A.; Choi, J.; Zhang, M.; Pacheco, J. L.; Abraham, J.; Bielejec, E.; Lukin, M. D.; Atatüre, M.; Lončar, M. Controlling the Coherence of a Diamond Spin Qubit through Its Strain Environment. *Nat. Commun.* **2018**, *9* (1), 2012–2012.
- (25) Meesala, S.; Sohn, Y.-I.; Pingault, B.; Shao, L.; Atikian, H. A.; Holzgrafe, J.; Gündoğan, M.; Stavrakas, C.; Sipahigil, A.; Chia, C.; Evans, R.; Burek, M. J.; Zhang, M.; Wu, L.; Pacheco, J. L.; Abraham, J.; Bielejec, E.; Lukin, M. D.; Atatüre, M.; Lončar, M. Strain Engineering of the Silicon-Vacancy Center in Diamond. *Physical Review B* **2018**, *97* (20), 205444–205444.
- (26) Wan, N. H.; Lu, T.-J.; Chen, K. C.; Walsh, M. P.; Trusheim, M. E.; De Santis, L.; Bersin, E. A.; Harris, I. B.; Mouradian, S. L.; Christen, I. R.; Bielejec, E. S.; Englund, D. Large-Scale Integration of Artificial Atoms in Hybrid Photonic Circuits. *Nature* **2020**, *583* (7815), 226–231.
- (27) Li, L.; Santis, L. D.; Harris, I. B. W.; Chen, K. C.; Gao, Y.; Christen, I.; Choi, H.; Trusheim, M.; Song, Y.; Errando-Herranz, C.; Du, J.; Hu, Y.; Clark, G.; Ibrahim, M. I.; Gilbert, G.; Han, R.; Englund, D. Heterogeneous Integration of Spin-Photon Interfaces with a CMOS Platform. *Nature* **2024**, *630* (8015), 70–76.
- (28) Lund-Hansen, T.; Stobbe, S.; Julsgaard, B.; Thyrrerstrup, H.; Sünner, T.; Kamp, M.; Forchel, A.; Lodahl, P. Experimental Realization of Highly Efficient Broadband Coupling of Single Quantum Dots to a Photonic Crystal Waveguide. *Phys. Rev. Lett.* **2008**, *101* (11), 1–4.
- (29) Dewhurst, S. J.; Granados, D.; Ellis, D. J. P.; Bennett, A. J.; Patel, R. B.; Farrer, I.; Anderson, D.; Jones, G. A. C.; Ritchie, D. A.; Shields, A. J. Slow-Light-Enhanced Single Quantum Dot Emission in a Unidirectional Photonic Crystal Waveguide. *Appl. Phys. Lett.* **2010**, *96* (3), 1–4.
- (30) Laucht, A.; Günthner, T.; Pütz, S.; Saive, R.; Frédérick, S.; Hauke, N.; Bichler, M.; Amann, M. C.; Holleitner, A. W.; Kaniber, M.; Finley, J. J. Broadband Purcell Enhanced Emission Dynamics of Quantum Dots in Linear Photonic Crystal Waveguides. *J. Appl. Phys.* **2012**, *112* (9). <https://doi.org/10.1063/1.4764923>.
- (31) Ba Hoang, T.; Beetz, J.; Midolo, L.; Skacel, M.; Lermer, M.; Kamp, M.; Höfling, S.; Balet, L.; Chauvin, N.; Fiore, A. Enhanced Spontaneous Emission from Quantum Dots in Short Photonic Crystal Waveguides. *Appl. Phys. Lett.* **2012**, *100* (6), 061122–061122.
- (32) Arcari, M.; Söllner, I.; Javadi, A.; Lindskov Hansen, S.; Mahmoodian, S.; Liu, J.; Thyrrerstrup, H.; Lee, E. H.; Song, J. D.; Stobbe, S.; Lodahl, P. Near-Unity Coupling Efficiency of a Quantum Emitter to a Photonic Crystal Waveguide. *Phys. Rev. Lett.* **2014**, *113* (9), 1–5.
- (33) Söllner, I.; Mahmoodian, S.; Hansen, S. L.; Midolo, L.; Javadi, A.; Kiršanskė, G.; Pregnolato, T.; El-Ella, H.; Lee, E. H.; Song, J. D.; Stobbe, S.; Lodahl, P. Deterministic Photon-emitter Coupling in Chiral Photonic Circuits. *Nat. Nanotechnol.* **2015**, *10* (9), 775–778.
- (34) Yoshimi, H.; Yamaguchi, T.; Katsumi, R.; Ota, Y.; Arakawa, Y.; Iwamoto, S. Experimental Demonstration of Topological Slow Light Waveguides in Valley Photonic Crystals. *Opt. Express* **2021**, *29* (9), 13441–13441.
- (35) Kuruma, K.; Yoshimi, H.; Ota, Y.; Katsumi, R.; Kakuda, M.; Arakawa, Y.; Iwamoto, S. Topologically-Protected Single-Photon Sources with Topological Slow Light Photonic Crystal Waveguides. *Laser & Photonics Reviews* **2022**, *16* (8), 2200077–2200077.
- (36) Ren, H.; Matheny, M. H.; MacCabe, G. S.; Luo, J.; Pfeifer, H.; Mirhosseini, M.; Painter, O. Two-

- Dimensional Optomechanical Crystal Cavity with High Quantum Cooperativity. **2019**, 1–21.
- (37) Guo, X.; Deegan, N.; Karsch, J. C.; Li, Z.; Liu, T.; Shreiner, R.; Butcher, A.; Awschalom, D. D.; Heremans, F. J.; High, A. A. Tunable and Transferable Diamond Membranes for Integrated Quantum Technologies. *Nano Lett.* **2021**, *21* (24), 10392–10399.
- (38) Guo, X.; Xie, M.; Addhya, A.; Linder, A.; Zvi, U.; Wang, S.; Yu, X.; Deshmukh, T. D.; Liu, Y.; Hammock, I. N.; Li, Z.; DeVault, C. T.; Butcher, A.; Esser-Kahn, A. P.; Awschalom, D. D.; Deegan, N.; Maurer, P. C.; Heremans, F. J.; High, A. A. Direct-Bonded Diamond Membranes for Heterogeneous Quantum and Electronic Technologies. *Nat. Commun.* **2024**, *15* (1), 8788.
- (39) Notomi, M.; Yamada, K.; Shinya, A.; Takahashi, J.; Takahashi, C.; Yokohama, I. Extremely Large Group-Velocity Dispersion of Line-Defect Waveguides in Photonic Crystal Slabs. *Phys. Rev. Lett.* **2001**, *87* (25), 253902–253902.
- (40) Khanaliloo, B.; Jayakumar, H.; Hryciw, A. C.; Lake, D. P.; Kaviani, H.; Barclay, P. E. Single-Crystal Diamond Nanobeam Waveguide Optomechanics. *Phys. Rev. X* **2015**, *5* (4), 1–21.
- (41) Chia, C.; Machielse, B.; Shams-Ansari, A.; Lončar, M. Development of Hard Masks for Reactive Ion Beam Angled Etching of Diamond. *Opt. Express* **2022**, *30* (9), 14189–14201.
- (42) Rogers, L. J.; Jahnke, K. D.; Teraji, T.; Marseglia, L.; Müller, C.; Naydenov, B.; Schaffert, H.; Kranz, C.; Isoya, J.; McGuinness, L. P.; Jelezko, F. Multiple Intrinsically Identical Single-Photon Emitters in the Solid State. *Nat. Commun.* **2014**, *5* (1), 4739–4739.
- (43) Castelletto, S.; Boretti, A. Silicon Carbide Color Centers for Quantum Applications. *JPhys Photonics* **2020**, *2* (2), 022001.
- (44) Redjem, W.; Durand, A.; Herzig, T.; Benali, A.; Pezzagna, S.; Meijer, J.; Kuznetsov, A. Y.; Nguyen, H. S.; Cuff, S.; Gérard, J.-M.; Robert-Philip, I.; Gil, B.; Caliste, D.; Pochet, P.; Abbarchi, M.; Jacques, V.; Dréau, A.; Cassabois, G. Single Artificial Atoms in Silicon Emitting at Telecom Wavelengths. *Nat. Electron.* **2020**, *3* (12), 738–743.

Supplementary Information:

**Purcell enhanced emissions from diamond color centers in
slow light photonic crystal waveguides**

1. Optical measurement setup

For the room-temperature PL measurement of the waveguide modes, we used a commercial spectrometer system (Horiba LabRam Evolution) with free-space off-resonance excitation and collection. The sample is excited with a continuous wave green diode laser (523 nm). The grating selected is 600 gr/mm.

For the low-temperature SiV measurements, we used a confocal setup, as shown in the simplified diagram Fig. S1. The supercontinuum pulsed laser is SuperK EXTREME with a repetition rate of 78 MHz. The 4 K cryo system is Attodry800, and the operating temperature is 5 K. We placed a short pass filter of 700 nm in front of the laser for the off-resonant excitation of the SiVs. A low-jitter NbN SNSPD with impedance-matching tapers and differential readout electronics is provided by our collaborators at JPL¹. The detectors are optimized for a peak efficiency at 775 nm, but the efficiency is still reasonably high at 737 nm. The spectrometer used is SpectraPro HRS-750, and the grating selected for the SiV spectra is 1800 gr/mm.

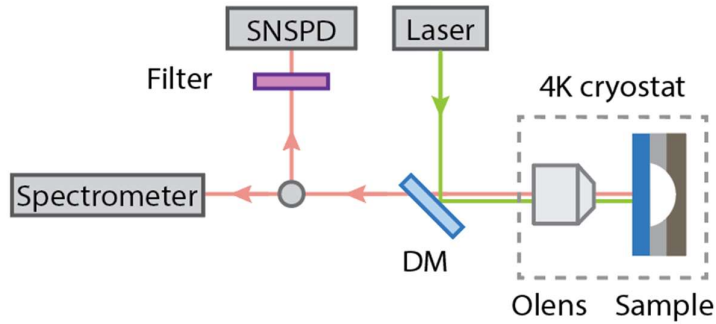


Fig. S1 Schematics of the SiV optical measurement setup. SNSPD: superconducting nanowire single-photon detector; DM: dichroic mirror, reflecting green and passing red; O lens: objective lens.

2. Measured Q factors (linewidth) of Fabry-Pérot peaks

Fig. S2 shows measured Q factors (linewidth) extracted from the observed Fabry-Pérot (FP) fringes shown in Fig. 3(b) in the main text. We fitted the FP peaks with multiple Lorentzian peak functions.

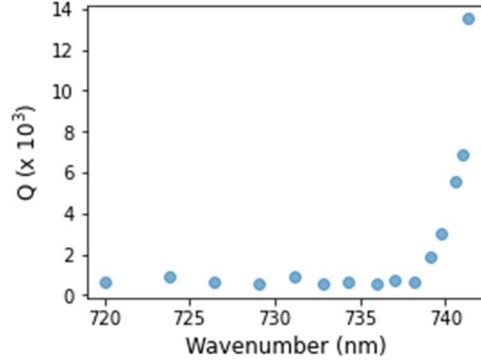


Fig. S2 Q factors for the FP resonance. The data points are extracted from the fitting of FP fringes in Fig. 3(b) in the main text.

3. Estimation of n_g corresponding to target SiV transition lines

Fig. S3 (a) and (b) show measured n_g for two waveguide devices with $a = 261$ nm (named waveguide 1 and 2) which were used for the SiV lifetime experiments in the main text. The theoretical curve is overlaid with the experimental data for better comparison. From the theoretical curve, we can estimate the corresponding n_g at the SiV transition lines (~ 737 nm) to be ~ 11 and ~ 20 for waveguide 1 and 2, respectively. The slight difference in position of the Brillouin zone edge of the waveguide modes between waveguide 1 and 2 could be due to fabrication imperfection.

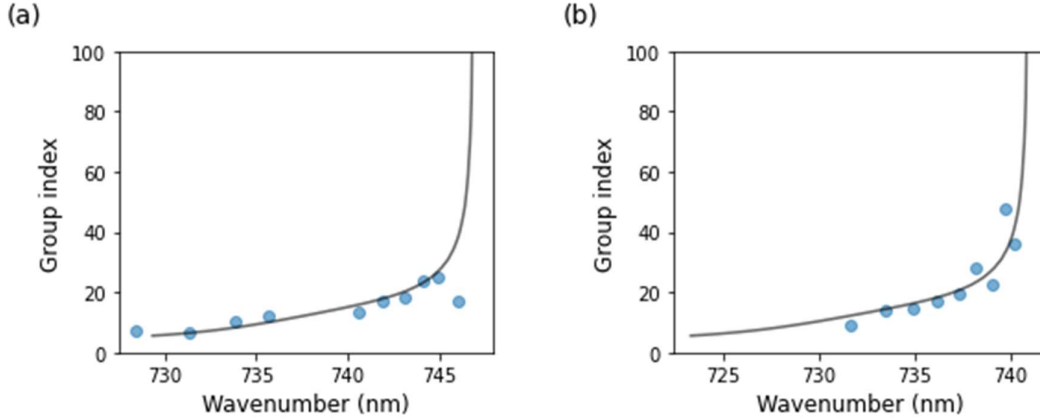


Fig. S3 Measured n_g as a function of wavelength measured for two waveguides with (a) a low n_g (~ 11) and (b) high n_g (~ 20) at ~ 737 nm. The dots are experimental data while the gray curve is the theoretical curve with an offset for comparison.

4. Second-order correlation measurements

Second-order correlation measurements are performed for a SiV in one of the PhC waveguides using a Hanbury Brown-Twiss setup equipped with two SNSPDs (Fig. S1). We off-resonantly excite the SiV in the PhC waveguide by a pulsed laser (SuperK EXTREME) and collect the PL emission from the C line of the SiV by using a spectral

filter with a bandwidth of ~ 50 GHz. The excitation power is 3.3 mW. Fig. S4 shows the intensity correlation histogram measured at 5K. The second-order correlation function at zero delay time, $g^2(0)$, exhibits an antibunching with a value of 0.47. The non-zero value of $g^2(0)$ could be due to the contribution of the PL emission of waveguide modes. We note that we also confirmed that single SiVs in other thin films that were fabricated using the same technique can exhibit the antibunching feature even in nanostructures ².

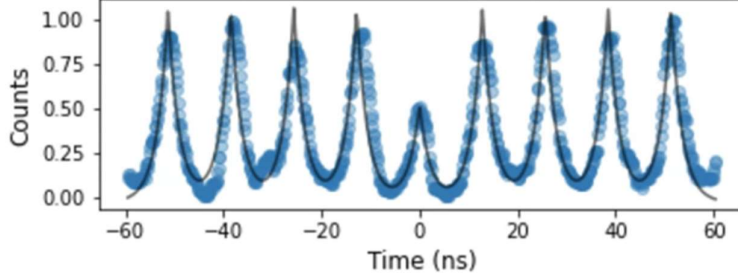


Fig. S4 Second-order correlation measurements. Normalized auto-correlation function $g^2(t)$ measured for a SiV in a PhC waveguide sample. The solid line corresponds to a fitting curve.

5. Calculation of Purcell factor

We estimate the Purcell factor of the investigated zero-phonon line (ZPL) F_{ZPL} using the following equation ³:

$$F_{ZPL} = (\tau_{off} / \tau_{on} - 1) / \zeta_{ZPL} \quad (S3)$$

Here ζ_{ZPL} is the fraction of the total emission into the ZPL visible at 4K for an SiV, which is estimated by a product of the Debye–Waller factor of 70%⁴ and the branching ratio of 32.5/45.2% into B/C transition at 4K³. For τ_{off} , we use the characteristic lifetime of a bulk SiV of 1.7 ns, which is also consistent with the measured SiV lifetime on this sample. For τ_{on} , we use the shortest measured lifetime of a SiV on the resonant waveguide of 1.01 ns.

6. Calculation of enhancement factor of SiV emission decay rate in waveguides

We consider a two-dimensional line-defect photonic crystal waveguide in diamond, shown in Fig.1 (a) in the main text (refractive index of the diamond slab $n = 2.4$). The waveguide supports transverse electric (TE) waveguide mode with a group index n_g . Under dipole approximation, the SiVs are assumed as point dipoles. The SiV emission decay rate into a waveguide mode Γ_{wg} normalized to the decay rate in bulk Γ_0 is calculated using the following equation ⁵:

$$\frac{\Gamma_{wg}}{\Gamma_0} = \frac{3}{4\pi} \frac{(\lambda/n)^2 n_g}{S_{eff} n} \frac{|E(r) \cdot d|^2}{|d|^2 |E_{max}|^2} \quad (S2)$$

Here, λ and d are the vacuum wavelength and electric dipole moment of the SiV, respectively. S_{eff} is the effective mode defined as:

$$S_{eff} = \iint n(r)^2 |E(r)|^2 d^2r / \max [n(r)^2 |E(r)|^2] \quad (S3)$$

The local electric field at a position r is defined as $E(r)$. We calculate the electric field of the waveguide modes by a 3D plane wave expansion method. We assume that the SiV is primarily coupled to the electric field of E_y to get a larger enhancement factor compared to E_x . To calculate the maximum achievable enhancement factor, we take into account a $\sim 30\%$ reduction due to the shallow implantation of the SiVs (~ 40 nm from the top surface, with an ion implantation dose of $\sim 10^8$) from the maximum electric field at the middle of the diamond slab (80 nm). We also consider the mismatch of the polarization between the local electric field (110) and SiV (111), resulting in an additional reduction of the factor by $\sim 34\%$.

7. Calculation of β factor

We roughly estimate the β factor using the following equation: $\beta = \gamma_{wg} / (\gamma_{wg} + \gamma_{PhC})$, where γ_{wg} and γ_{PhC} are the emission rate of SiVs in a waveguide and in photonic crystals (PhCs). We use the measured emission rate of the SiV in a waveguide (~ 0.83 ns $^{-1}$) for γ_{wg} . For γ_{PhC} , we use the previously reported value of ~ 0.38 ns $^{-1}$ in 2D PhC⁶. In this calculation, we do not include the emission decay into the phonon sideband and non-radiative transitions.

8. Estimation of achievable β factor

Fig. S5 shows the calculated n_g (top), Fp (middle), and β (bottom) for electric field E_y , considering the polarization mismatch between a SiV dipole and the local electric field. We assume that the SiV is coupled to the maximum electric field. For the calculation of β , we use the equation of β in section 7, using $\gamma_{wg} = Fp \gamma_{bulk}$ (bulk rate $\gamma_{bulk} = 0.59$ ns $^{-1}$) and $\gamma_{PhC} \sim 0.38$ ns $^{-1}$. For the experimentally achievable value of $n_g = 70$ shown in Fig. 3 in the main text, we can estimate the achievable $Fp = 9.4$ and $\beta = 94.3\%$, respectively.

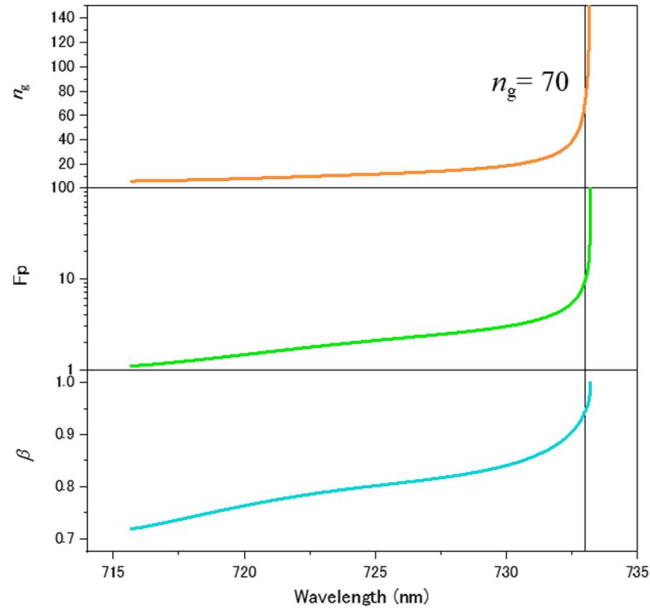


Fig. S5 Calculated n_g (top), F_p (middle), and β (bottom) when the SiV is coupled to the electric field of E_y . The vertical line represents the wavelength for $n_g = 70$, corresponding to $F_p = 9.4$ and $\beta = 0.943$.

References

- (1) Colangelo, M.; Korzh, B.; Allmaras, J. P.; Beyer, A. D.; Mueller, A. S.; Briggs, R. M.; Bumble, B.; Runyan, M.; Stevens, M. J.; McCaughan, A. N.; Others. Impedance-Matched Differential Superconducting Nanowire Detectors. *Physical Review Applied* **2023**, *19* (4), 044093.
- (2) Ding, S. W.; Haas, M.; Guo, X.; Kuruma, K.; Jin, C.; Li, Z.; Awschalom, D. D.; Deegan, N.; Heremans, F. J.; High, A. A.; Loncar, M. High-Q Cavity Interface for Color Centers in Thin Film Diamond. *Nat. Commun.* **2024**, *15* (1), 6358–6358.
- (3) Zhang, J. L.; Sun, S.; Burek, M. J.; Dory, C.; Tzeng, Y.-K.; Fischer, K. A.; Kelaita, Y.; Lagoudakis, K. G.; Radulaski, M.; Shen, Z.-X.; Melosh, N. A.; Chu, S.; Lončar, M.; Vučković, J. Strongly Cavity-Enhanced Spontaneous Emission from Silicon-Vacancy Centers in Diamond. *Nano Letters* **2018**, *18* (2), 1360–1365.
- (4) Aharonovich, I.; Castelletto, S.; Simpson, D. A.; Su, C.-H.; Greentree, A. D.; Prawer, S. Diamond-Based Single-Photon Emitters. *Rep. Prog. Phys.* **2011**, *74* (7), 076501.
- (5) Quan, Q.; Bulu, I.; Lončar, M. Broadband Waveguide QED System on a Chip. *Phys. Rev. A* **2009**, *80* (1), 011810.
- (6) Riedrich-Möller, J.; Arend, C.; Pauly, C.; Mücklich, F.; Fischer, M.; Gsell, S.; Schreck, M.; Becher, C. Deterministic Coupling of a Single Silicon-Vacancy Color Center to a Photonic Crystal Cavity in Diamond. *Nano Lett.* **2014**, *14* (9), 5281–5287.

